O_2 Activation in a Dinuclear Fe(II)/EDTA Complex: Spin Surface Crossing As a Route to Highly Reactive Fe(IV)oxo Species†

Paola Belanzoni,*,‡ Leonardo Bernasconi,*,§,∥ and Evert Jan Baerends*,§,⊥

Department of Chemistry, University of Perugia, via Elce di Sotto 8, 06123 Perugia, Italy, Theoretical Chemistry Section, Vrije Universiteit Amsterdam, De Boelelaan 1083, 1081 HV Amsterdam, The Netherlands, Science and Technology Facilities Council Rutherford Appleton Laboratory, Harwell Science and Innovation Campus, Didcot, Oxfordshire, OX11 0QX United Kingdom, and Department of Chemistry, Pohang University of Science and Technology, Pohang 790-784, South-Korea

Received: April 12, 2009; Revised Manuscript Received: June 13, 2009

We study the cleavage of O_2 in gas phase $[(EDTAH)Fe(O_2)Fe(EDTAH)]^{2-}$, a proposed intermediate in the aqueous Fe(II)-to-Fe(III) autoxidation reaction in the presence of atmospheric dioxygen and EDTA ligand. The role of the exchange coupling between the locally high-spin Fe centers in the O−O dissociation is investigated. Using results from broken symmetry (BS) density functional theory (DFT) calculations, we show that the system can be modeled as two high-spin (HS) $S = 5/2$ Fe(III) d^5 centers coupled through a bridging peroxo O_2^{2-} ligand, consistent with hypotheses advanced in the literature. We show that in this electronic configuration the O−O cleavage reaction is forbidden by (spin) symmetry. Dissociation of the O_2^{2-} group to the product ground state may only take place if the system is allowed to undergo a transition to a state of lower spin multiplicity ($S = 4$) as the O−O bond is stretched. We show that the exchange coupling between the two Fe ions in $[(EDTAH)Fe(O_2)Fe(EDTAH)]^{2-}$ plays only a minor role in defining the chemistry of O_2 activation in this system. The peroxo/oxo interconversion involves a state outside the Heisenberg spin ladder of the initial $S = 5$ state. In this $S = 4$ state, the dinuclear complex evolves to two oxo complexes, $[EDTAH\cdot Fe(IV)O]^-$, with an overall energy barrier of only ∼86 kJ mol^{-1}. According to recent theoretical work, the latter species are exceptionally strong oxidants, making them ideal candidate catalysts for organic oxidations (including C−H bond hydroxylation). We highlight the (spin) symmetry forbidden nature of the reaction on the $S = 5$ surface and its symmetry allowed character in the electronic configuration with $S = 4$.

I. Introduction

Fe(IV)-oxo (ferryl) intermediates have been shown to play an extremely important role in a number of enzymatic processes involved in aerobic biochemistry,[1–14] in which they act as powerful oxidants for unreactive substrates, including saturated hydrocarbons.[15–28] Nonheme enzymes containing divalent or trivalent dinuclear transition metal ion active sites are known to generate ferryl intermediates by direct activation and reduction of atmospheric dioxygen.[13,14,29] Well known and extensively studied examples of this class of metalloproteins are methane monooxygenase (MMO)[29,30] and ribonucleotide reductase,[31] containing dinuclear iron centers, and tyrosynase,[32] containing dinuclear copper centers. In the two former systems, the activation of dioxygen is brought about by reduction of O_2 in an initial $Fe(II)O_2$ Fe(II) adduct to a ferric-peroxo $Fe(III)O_2^{2-}$ Fe(III) complex. Subsequent homolytic cleavage of the O−O bond leads to the generation of an Fe-(μ-O)$_2$-Fe diamond core, with various Fe−O distances and orientations of the O−O fragment with respect to the Fe−Fe axis being reported. The compound Q of MMO has this type of structure. Such a complex can act as hydroxylation catalyst by transferring an oxygen atom either directly, or via a rebound mechanism.[2,33,34] The surrounding protein medium has been proposed to play a crucial role in promoting O_2 bond cleavage and stabilizing reactive intermediates.[29,31,35,36]

Similar reactions may play a role in the abiotic Fe based oxidation chemistry, where high-valent Fe catalysts for aliphatic hydroxylation are very important. At present, the controlled inorganic generation of ferryl species from Fe(II)/Fe(III) ions in aqueous or nonaqueous solvents from direct activation of atmospheric dioxygen remains an ambitious, if extremely far reaching, objective. Ferryl species have conclusively been proven to be generated in aqueous solution at room temperature and pressure conditions from the reaction of Fe(II) with O_3,[37–39] and increasing evidence[20,22,39–42] is being put forward that a ferryl species, namely $[Fe(IV)O\cdot(H_2O)_5]^{2+}$, might be the long sought after active intermediate in aqueous Fenton chemistry.[2,33,34,43–46]

Recently, experimental work on the autoxidation reaction of Fe(II) to Fe(III) in aqueous solution in the presence of dioxygen and EDTA ligand (in various of its possible protonation states) has provided evidence for the generation of non radical intermediates sufficiently reactive to oxidize alcohols, and even to decompose the EDTA ligand.[47–50] It has been proposed that, in normal experimental conditions, dioxygen activation and its reduction to two oxide ions may occur through a mechanism essentially analogous to the one observed in the Fenton mixture, *via* the intermediate generation of H_2O_2, which may then oxidize Fe(II) to Fe(IV).[47,49] Alternatively,[51] dioxygen reduction to two oxide ions might be thought to occur through a mechanism

† Part of the "Walter Thiel Festschrift".

* To whom correspondence should be addressed. E-mail: paola@thch.unipg.it; L.Bernasconi@rl.ac.uk; EJ.Baerends@few.vu.nl.

‡ University of Perugia.

§ Vrije Universiteit Amsterdam.

∥ Science and Technology Facilities Council Rutherford Appleton Laboratory.

⊥ Pohang University of Science and Technology.

10.1021/jp9033672 CCC: $40.75
Published on Web 07/14/2009

essentially analogous to the one observed in biological systems, namely the coordination of dioxygen in a bridging position between two Fe centers, followed by reduction to two EDTA-chelated Fe(IV)-oxo complexes, which can potentially act as active species in the oxidation of solvated organics.[13,14,30] Both mechanisms are compatible with the multistep model for the aqueous Fe(II)-to-Fe(III) autoxidation reaction in the presence of EDTA proposed by van Eldik and co-workers on the basis of reaction kinetic measurements.[52–55]

Although no conclusive evidence has been put forward to date for the actual involvement of ferryl species in Fe(II)/O_2/EDTA chemistry, these experimental findings may provide the first known example of a genuinely abiotic system in which highly reactive ferryl intermediates are generated at ambient conditions from direct activation of dioxygen. As such, they may pave the way for the design of completely new classes of Fenton-like reagents[15,23,26,56–60] for organic hydroxylations, involving readily available reactants, simple and safe synthetic processes, and mild working conditions. Interestingly, theoretical results seem to indicate that EDTA-ferryl complexes may possess C−H activation properties comparable, if not superior, to any synthetic ferryl system know to date.[61] This fact is largely a consequence of the peculiar coordination of the Fe(IV)O group when chelated by EDTA, with up to four oxygen atoms in equatorial position (i.e., in the plane perpendicular to the Fe−O bond), and a virtually free axial coordination site protected from attack of solvent molecules by the EDTA cage. This coordination geometry has been predicted to be particularly effective in enhancing the catalytic properties of the ferryl group,[62] through a selective stabilization of the $3\sigma^*\alpha$ orbital which, acting as an acceptor of electrons from a substrate, is responsible for the unusual reactivity of Fe(IV)O systems in the hydroxylation of hydrocarbons.[22,26,62,63]

In a recent theoretical study of the electronic structure of gas phase Fe(II)/EDTAH_n/O_2 complexes,[51,61] two of us pointed out a series of striking similarities between the structure of the $[(EDTAH)Fe(O_2)Fe(EDTAH)]^{2-}$ complex, the postulated peroxo intermediate in the van Eldik Fe(II)-to-Fe(III) autoxidation reaction,[52–55] and those of the dinuclear Fe intermediates **P** and **Q** of methane monooxygenase and ribonucleotide reductase.[29–31] We also proved that the constrained homolytic cleavage of the O−O bond may indeed lead to the generation of two $[(EDTAH)FeO]^-$ systems with an overall reaction energy barrier of ~66 kJ mol^{-1}, a value which is very close to the O−O cleavage barrier computed by Siegbahn for the conversion of compound **P** into compound **Q** in methane monooxygenase (71.5 kJ mol^{-1}).[31] However, the O−O cleavage in $[(EDTAH)Fe(O_2)Fe(EDTAH)]^{2-}$ was found to involve a transition from an initial $S = 5$ ground spin state to a final $S = 4$ state, occurring at or just before the transition state, rather than to take place on a single spin energy surface ($S = 5$) with a subsequent transition to a singlet state, as happens in methane monooxygenase. According to our results, $[(EDTAH)Fe(O_2)Fe(EDTAH)]^{2-}$ thus evolves from an O_2 bridged dinuclear system to a pair of high spin ($S = 2$) ferryl complexes. This fact is particularly important for the reactivity of the resulting ferryl complexes, since, as shown in ref.[62] based on calculations and extensively confirmed experimentally, of the two low-energy spin states of ferryl compounds, triplet ($S = 1$) and quintet ($S = 2$), the latter is by far the most reactive. This has been explained as a consequence of the lower orbital energy of the most important acceptor orbital, the $3\sigma^*\alpha$, when stabilized by the strong exchange field of four unpaired spin electrons[62,63] (see also Decker et al.[26]).

In this work we will study in greater detail the role of the magnetic ("exchange") coupling between Fe centers in $[(EDTAH)Fe(O_2)Fe(EDTAH)]^{2-}$, in an attempt to understand if and how this weak interaction may play a role in promoting or hindering the cleavage of the O−O bond. The simplest representation of the $[(EDTAH)Fe(O_2)Fe(EDTAH)]^{2-}$ complex, from this perspective, is that of a (nonspin polarized) peroxo species, O_2^{2-}, bridging 2 HS Fe(III) centers (d^5, $S = 2.5$). Within this idealized picture, a whole set of spin states can be generated ("Heisenberg spin ladder"), with S varying between $S = S_1 + S_2 = 5$ and $S = S_1 + S_2 = 0$ in steps of $\Delta S = -1$. The same applies to all other spin surfaces, including, in particular, the $S = 4$ surface. Is the $S = 5 \rightarrow S = 4$ spin transition during O−O stretching in any way related to the exchange coupling? Or does the lower activation barrier on the $S = 4$ surface rather involve predominantly a change in the occupation of the spatial orbitals?

We will address these questions using calculations based on the BS approach[64–69] within DFT. This method has been proven in several situations to yield an appropriate description of the interaction between localized spins, as well as to allow reasonably accurate estimates of exchange coupling constants between the interacting ions.[69–73] We will conclude that the different spin states that belong to the Heisenberg ladder of exchange coupled states do not behave differently in the process of O−O bond breaking: exchange coupling is basically always weak on the energy scale relevant for chemical processes like bond breaking. It will be important to see how a different orbital occupation, which entails the involvement of a state outside a given Heisenberg ladder, is essential for lowering the cleavage barrier, as compared to an exclusive involvement of states belonging to the same ladder: within the same ladder of states the interconversion Fe(III)-O_2^{2-}-Fe(III) ⇌ Fe(IV)O···OFe(IV) is always a symmetry forbidden reaction. This is in keeping with the well-known fact that it is the nature of occupied orbitals (in particular their bonding or antibonding character) that determines the overall chemical reactivity. A change in occupation, with a concomitant change in spin multiplicity, allows the peroxo bridge in $[(EDTAH)Fe(O_2)Fe(EDTAH)]^{2-}$ to evolve smoothly into two oxo units as the O−O distance increases. The occupation change is a necessary condition for the O−O cleavage in this system to occur with an energy barrier comparable to those estimated in biological O_2 activation processes, and therefore to make this process potentially important at ambient conditions.

The paper is organized as follows. In section II details regarding the calculations are provided. In section IIIA we analyze the magnetic coupling within the spin unrestricted BS approach, by calculating the Heisenberg coupling constants between the two Fe centers and the energy order of the spin states (ferromagnetically or antiferromagnetically ordered) along the O−O distance for the spin ladder ranging from state $S = 5$ to $S = 0$ (i.e., the sign of the Heisenberg coupling constant J). We find that the exchange coupling has virtually no effect on the O−O bond breaking. In section IIIB we give an electronic structure analysis of the O−O bond breaking process. We clarify why the excitation to the $S = 4$ state is important for making the O−O bond breaking a process with a relatively low barrier, that yields two ferryl ions (high-spin iron oxo) coordinated by $EDTAH^{3-}$ as product. The conclusions are summarized in section IV.

II. Computational Details

The Amsterdam density functional (ADF) package[74–76] was used for calculations with a TZP basis set for all atoms. The

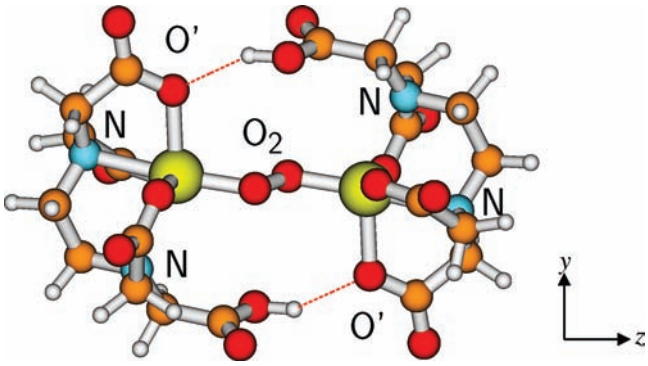

Figure 1. Structure of the reactant, the initial O_2 bridged dinuclear iron EDTAH^{3-} complex at d(O−O) = 1.352 Å. The Fe−Fe axis is parallel to the z axis, O_2 lies in the xz plane, which is perpendicular to the plane of drawing, and the y axis is the vertical in the plane of drawing (Fe−O′ is approximately along the y axis).

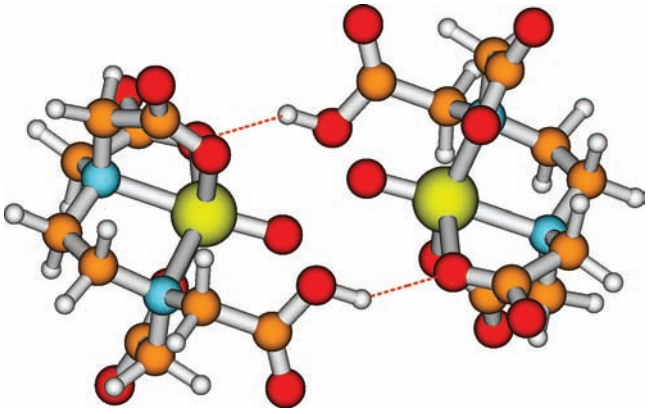

Figure 2. Structure of the product on the $S = 4$ surface: two EDTAH^{3-} coordinated FeO^{2+} ferryl ions connected by two hydrogen bonds.

inner core orbitals (3p for Fe, 1s for C, N, and O) were treated by the frozen core approximation. Relativistic effects were included by using the zero-order regular approximation (ZORA).[77,78] All calculations were performed in the spin-unrestricted approach using the OPBE functional, a combination of the OPTX and the PBE functionals[79,80] OPBE has been shown to yield spin state relative stabilities comparable to hybrid and *meta*-GGA functionals.[81–83] The BS[64,65] approach was employed to model the antiferromagnetic coupling between the Fe sites. In both $S = 5$ and $S = 4$ [(EDTAH)Fe(O_2)Fe(EDTAH)]$^{2-}$ optimized geometries the two Fe centers and the dioxygen molecule lie exactly in a plane. This allows us to adopt the following convention for the orientation of the coordinate system (see Figure 1).[51] We indicate as z the axis passing through the two Fe centers, with the origin at the middle point of the O−O bond. The xz plane corresponds to the Fe−O_2−Fe plane, and the y axis contains one coordinating O from the EDTAH ligand. O_2 is coordinated to the two metal ion centers in a geometry that is intermediate between end-on (η^1) and side-on (η^2): the angle α of the O−O axis with the z axis is 43.7°, the O−O distance is 1.352 Å in the $S = 5$ HS state (and 1.359 Å in the $S = 4$ state) (see Scheme 2 for geometric information). After O−O dissociation, the two [EDTAHFeO]$^-$ complexes are held together by hydrogen bonds, see Figure 2. The Fe−O··· O−Fe core still lies in the xz plane, now with a much longer O−O distance (2.059 Å), the Fe−O bonds shorten to 1.637 Å and define angles of 30.7° with the Fe−Fe (z) axis. Dissociation on the $S = 5$ surface leads to an entirely different product, namely an asymmetric coordination of stretched O_2 (rather than two oxo groups) to a single Fe, the bond with the other Fe being virtually broken. This is shown in Figure 3. The population analysis discussed below will be based on the neutral Fe atomic orbitals (a transformation of the primitive STO basis set) and the molecular orbitals of the superoxo O_2^- molecule in the $(1\sigma_g)^2(1\sigma_u)^2(2\sigma_g)^2(2\sigma_u)^2(3\sigma_g)^2(1\pi_u)^4(1\pi_g)^3(3\sigma_u)^0$ configuration (a transformation of the primitive STO basis set on the oxygens). Using orbitals from realistic fragments in the analysis reduces the dependence on the choice of primitive basis, a well-known limitation of standard Mulliken population analysis. We will henceforth denote the $1\pi_g$ as π^* and the $3\sigma_u$ as σ^*.

III. Results and Discussion

A. Exchange Coupling and the O−O Bond Breaking. ***1. Calculation of the Heisenberg Coupling Constant with the BS-DFT Approach: E_{HS} and E_{BS}.*** We consider the [(EDTAH)Fe(O_2)Fe(EDTAH)]$^{2-}$ complex in the gas phase. Here, and in the rest of this work, we will adopt optimized geometries computed at the OPBE level for various values of the O−O distance along the bond cleavage path (see ref 51 for further details). The simplest representation of the system at equilibrium before O−O bond breaking (d(O−O) = 1.352 Å, Figure 1) is in terms of two high spin Fe centers (both Fe(III) d^5) magnetically coupled through a closed shell O_2^{2-} bridge. We will consider below how close this description is to the actual situation, in terms of charge and spin density distributions. The maximum allowed value of S for this system is $S = S_1 + S_2 = 5$, with each Fe having five unpaired electrons in the 3d orbitals.

The state with maximum M_S value (indicated as HS state), $|S,M_S\rangle = |5,5\rangle$, can be represented by a single determinant with the largest number of up-spin orbitals occupied, as shown in Scheme 1 panel 1a. For this state, calculations can be performed under inversion symmetry, since Fe^1 and Fe^2 are equivalent and both have all spins up. Besides, this is a pure spin state, in which the Fe centers with spin $S_1 = 5/2$ and $S_2 = 5/2$ are coupled with all spins parallel, $|S_1S_2;S = 5,M_S = 5\rangle$. The remaining states belonging to the Heisenberg ladder originate from all the possible couplings between the two Fe centers, each carrying a spin $S_{1,2} = 5/2$, giving values of S between $S_{max} = 5$ and $S_{min} = 0$. These states differ only in the spin occupations of the ten spatial 3d orbitals.

The spacing between the energy levels of the states in the Heisenberg ladder is traditionally expressed in terms of the Heisenberg coupling operator, $J\hat{S}_1\cdot\hat{S}_2$. In the BS approach,[65] the Heisenberg coupling constants J can be computed from the HS and BS energies, E_{HS} and E_{BS} respectively, alone. E_{BS} is obtained by removing all symmetry elements relating the two metal ions, and forcing the spins to have antiparallel orientations on the two magnetic centers, cf. Scheme 1, panel 1b. This spin configuration can be expressed as a linear combination of the $M_S = 0$ components of all the Heisenberg spin states, but it is heavily weighted toward the $|S = 0, M_S = 0\rangle$ overall spin state. Noodleman[65,68] showed that the Heisenberg coupling constant can be obtained to good approximation from the relation

$$E_{HS} - E_{BS} = (-4J)S_1S_2 \qquad (1)$$

provided the magnetic coupling is weak. The energy ordering is given by the sign of J, whereas the magnitude of J determines the energy spacing of the spin states. The BS-DFT approach relies on the assumption that HS and BS spin configurations describe magnetic centers that are weakly coupled by a closed shell bridging ligand. We will now

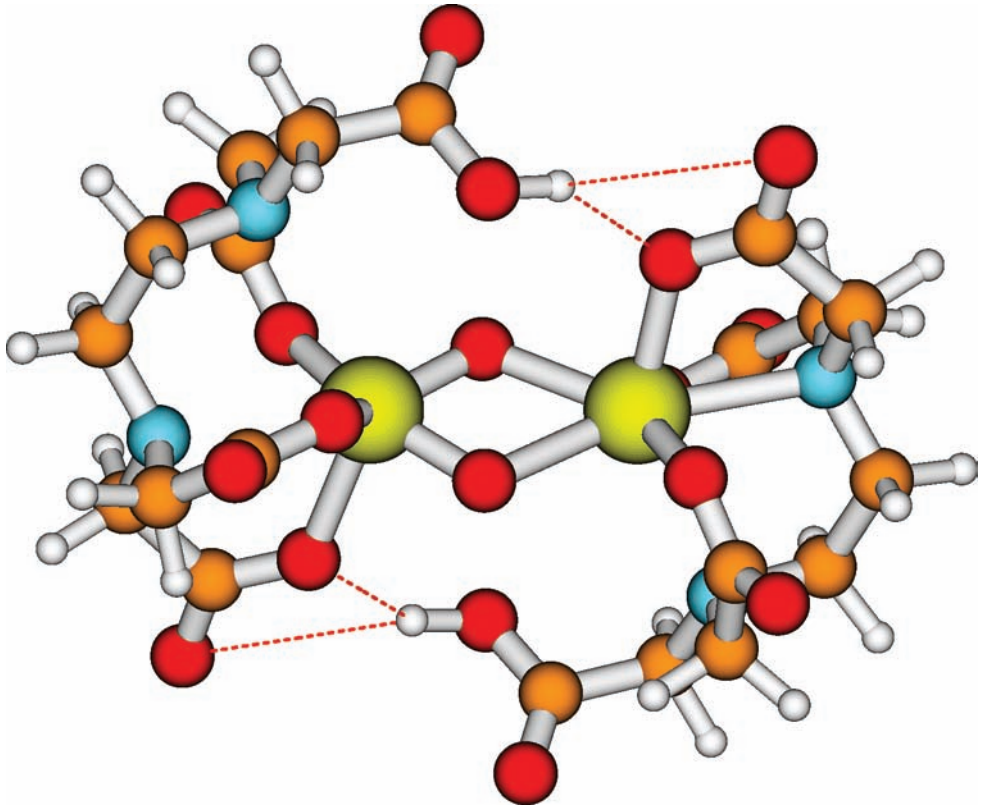

Figure 3. Structure of the high energy product of O_2 dissociation on the $S = 5$ surface: the broken O−O bond leads to asymmetric coordination of O_2 to the two Fe centers.

SCHEME 1: Schematic Representation of the Electronic Configuration of Two Fe d^5 Centers and a Bridging O_2^{2-} (Peroxo) in HS (1a) and BS (1b) Coupling, Compared to Two Fe d^6 Centers and an Intermediary Triplet O_2 (1c). Panel (1d): an Intermediate Situation with Partial Delocalization of the β Spins Over O_2 and the Fe Centers. Panel (1e): a Different Electronic Configuration, with a Superoxo O_2^- and a Mixed Valence Fe(II)−Fe(III) Pair, in the (Symmetrical) HS Coupling, with the Doublet O_2^- Spin Coupled Antiparallel to the Main Spin Direction

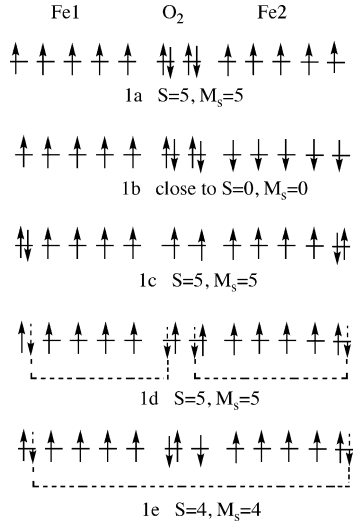

examine in some detail to what extent this is a correct description of the electronic structure of the $[(EDTAH)Fe(O_2)Fe(EDTAH)]^{2-}$ dinuclear complex.

*2. **HS State.*** The schematic spin distribution for the HS state is represented in Scheme 1, panel 1a. The actual situation is however far from being as clear-cut as depicted in the Scheme. In the bare $[Fe(II)EDTAH]^-$ complex there is a Fe(II) (d^6) center in a high spin ($S = 2$) configuration (four unpaired spins, two spins pair up in the d_{xz} orbital, see ref 51). When the O_2 molecule coordinates to the two Fe(II) centers, the spins of the triplet ($S = 1$) O_2 diradical can orient parallel to the $S = 2$ spin states of the Fe centers, to give an overall $S = 5$, $M_S = 5$ state (see Scheme 1, panel 1*c*). If the three fragments were far apart (noninteracting distance), this situation would be distinguishable from the Fe(III)-O_2^{2-}-Fe(III) arrangement within the $[(EDTAH)Fe(O_2)Fe(EDTAH)]^{2-}$ in the equilibrium geometry. The two situations would also obviously differ in their total energy. However, when the O_2 fragment and the two $[FeEDTAH]^-$ complexes are at interacting distance, the two states described by these different electronic configurations interact, and form two new mixed states. The lowest energy state is a mixture of the spin configurations depicted in panels 1a and 1c of Scheme 1. Of course, the model of these two interacting configurations (which could be cast in a VB form) is only useful when the interaction is fairly weak. But we can understand from this model that the actual ground state Kohn−Sham calculations, which should provide the exact ground state density for the mixed state, will have a charge distribution that is in between the extremes of pure peroxo and neutral. Such a charge distribution is established in the Kohn−Sham MO calculations by orbital mixing. The configuration mixing is reflected in the d orbitals admixing some character from O_2 orbitals with appropriate symmetry. This orbital mixing may vary from very strong (O_2 resembling O_2^{2-}, see Scheme 1, panel 1a) to very

TABLE 1: Mulliken Population Analysis for $[(EDTAH)Fe(O_2)Fe(EDTAH)]^{2-}$ at $d(O-O) = 1.352$ Å with Two High Spin Fe(II) Centers ($S^1 = S^2 = 5/2$) Coupled Ferromagnetically (Top: HS, $M_S = 5$) and Antiferromagnetically (Bottom: BS, $M_S = 0$)

HS, $S^1 = S^2 = 5/2$, $M_S = 5$				
	spin α		spin β	
	Fe^1	Fe^2	Fe^1	Fe^2
$3d_{z^2}$	0.99	0.99	0.30	0.30
$3d_{x^2-y^2}$	0.99	0.99	0.19	0.19
$3d_{xy}$	0.99	0.99	0.15	0.14
$3d_{xz}$	0.99	0.99	0.19	0.19
$3d_{yz}$	0.99	0.99	0.23	0.23
gross 3d pop.	5.05	5.05	1.12	1.12
		dioxygen		
π^*_x		0.95		0.56
π^*_y		0.96		0.52
gross pop.		6.80		5.86
charge	Fe	1.09	O_2	−0.70

BS, $S^1 = S^2 = 5/2$, $M_S = 0$				
	spin α		spin β	
	Fe^1	Fe^2	Fe^1	Fe^2
$3d_{z^2}$	0.99	0.31	0.31	0.99
$3d_{x^2-y^2}$	0.99	0.19	0.20	0.99
$3d_{xy}$	0.99	0.14	0.14	0.99
$3d_{xz}$	0.99	0.19	0.19	0.99
$3d_{yz}$	0.99	0.25	0.24	0.99
gross 3d pop.	5.04	1.14	1.14	5.04
		dioxygen		
π^*_x		0.74		0.74
π^*_y		0.72		0.73
gross pop.		6.32		6.32
charge	Fe	1.09	O_2	−0.68

weak, as in Scheme 1, panel 1c. Intermediate mixings, as shown in Scheme 1 panel 1d, may more realistically represent the actual situation.

Mulliken population analysis (Table 1, upper panel) shows that both Fe atoms have 5 unpaired electrons, with all spins up. The β spin d orbitals are however also partially occupied, because of orbital interaction with occupied orbitals localized on O_2^{2-} and on the $EDTAH^-$ ligands. This demonstrates that a considerable transfer of electron charge to the Fe ions is effectively taking place, which originates from both O_2^{2-} (predominantly the $\pi^*\beta$ orbitals, that lose about 1 electron in total) and the negatively charged ligands. The overall charge on O_2 is −0.70.

A MO energy diagram of this situation is shown in Figure 4. The energies of the 10 dα orbitals (plus and minus combinations of the dα orbitals on the Fe atoms) are lowered by the large exchange stabilization. These orbitals, which also show substantial mixing with various $EDTAH^{3-}$ orbitals, appear at the bottom (left side) of the figure. They are all fully occupied (0.99 electrons per d orbital, see Table 1). The "empty" dβ counterparts are at much higher energy, and well within the unoccupied region of the spectrum (see Figure 4, right side). Orbitals with predominant O_2 π^* character are located just between the dα and dβ sets. Their orbital compositions and energies are given in Table 2. The orbitals 130aα and 131aα, and 120aβ and 121aβ are predominantly O_2 π^* orbitals (percentages vary from 53 to 87%), with only some very small d character admixed. These orbitals are destabilized by orbital repulsion with the low-lying occupied dα orbitals. This being an occupied-occupied orbital interaction, the original $\pi^*\alpha$ orbitals retain approximately their full occupation (0.95 electrons, see Table 1). The empty dβ

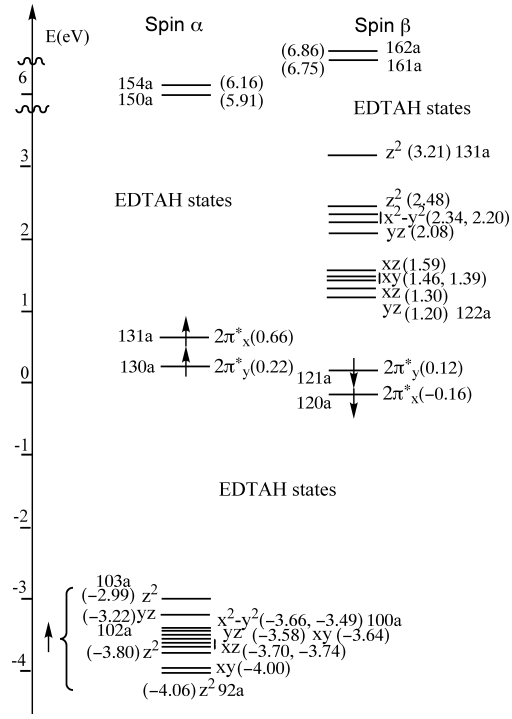

Figure 4. Orbital energy diagram for the symmetrical HS situation, with all dα orbitals on both irons occupied (and forming + and − combinations by symmetry). All dβ orbitals are unoccupied.

orbitals are higher lying, and they stabilize the $\pi^*\beta$ orbitals slightly. The latter interaction indicates that electrons are being transferred to the Fe dβ orbitals, with the $\pi^*\beta$ orbitals losing approximately 0.90 electrons (which would correspond to a charge of −1.10 electrons on O_2). This interaction is attractive (donor−acceptor ($\pi^*\beta \rightarrow d\beta$) interaction), and it is the one responsible for the $Fe-O_2-Fe$ bonding. This is in agreement with the $Fe-O_2-Fe$ bonding as described by Brunold et al.[84] for a model complex of methane monooxygenase, $(NH_3)_3Fe(O_2)(O_2CH)_2Fe(NH_3)_3$ in which the two Fe ions are bridged by carboxylate bridges.

The actual total charge on O_2 (−0.70 electrons, Table 1) is substantially less negative than this predicted value of −1.10. This is explained by the involvement of additional O_2 orbitals, which bring the total charge donated to Fe by O_2^{2-} to 1.30 electrons, i.e., 0.65 el. per Fe. The Fe dβ on one iron ion acquire much more than the 0.65 el. that O_2^{2-} has lost, namely 1.12 el. The additional electronic charge in Fe dβ comes from the N and O atoms of the $EDTAH^{3-}$ ligands. Considering as reference O_2^{2-} (peroxo) and Fe^{3+} (Fe(III)) charges, the calculated charge of Fe (+1.09) indicates that each of the Fe ions receives a total of 1.91 el., considerably more than the 1.12 el. going into the Fe dβ. This additional electronic charge is likely to be partially delocalized on the diffuse 4s and 4p orbitals.

Based on this analysis, we conclude that, with 0.65 electrons moving from O_2^{2-} to the dβ orbitals of each Fe, the picture of Scheme 1, panel 1d, offers perhaps the most realistic representation of the actual spin and charge distribution. Therefore, the accepted description[52–55] of the $[(EDTAH)Fe(O_2)Fe(EDTAH)]^{2-}$ core as composed of two HS Fe(III) ions with five unpaired α spin electrons, coupled through a "closed shell" O_2^{2-} ion, is essentially tenable. The slightly idealized nature of this description should nonetheless be kept in mind. Within this model for the HS configuration, the exchange coupling interaction generates a series of spin states (Heisenberg ladder) with $S = 0 - 5$ and $\Delta S = \pm 1$.

TABLE 2: Energies (eV) and Composition (%) of Selected Unoccupied and Occupied Spin-down/Spin-up Molecular Orbitals of $[(EDTAH)Fe(O_2)Fe(EDTAH)]^{2-}$ at $d(O-O) = 1.352$ Å on the $S = 5$ Spin Surface (HS)

HS (symmetric) $S^1 = S^2 = 5/2$, $S = 5$, d(O−O) = 1.352 Å											
			Fe					dioxygen			
level		energy	$d_{x^2-y^2}$	d_{xz}	d_{yz}	d_{xy}	d_{z^2}	4s	π_x^*	π_y^*	σ^*
					Unoccupied						
4s	162aβ	6.861	0	0	0	0	0	18	0	0	17
4s	161aβ	6.747	0	0	0	0	0	15	0	0	5
4s	154aα	6.157	0	0	0	0	0	13	0	0	13
4s	150aα	5.905	0	0	0	0	0	16	0	0	22
$d_{z^2} + d_{z^2}$	131aβ	3.208	4	0	18	0	37	0	13	9	0
$d_{z^2} - d_{z^2}$	130aβ	2.483	16	0	14	2	43	0	0	0	0
$d_{x^2-y^2} + d_{x^2-y^2}$	129aβ	2.340	35	0	0	15	7	0	8	18	0
$d_{x^2-y^2} - d_{x^2-y^2}$	128aβ	2.197	32	4	13	21	0	0	0	0	0
$d_{yz} + d_{yz}$	127aβ	2.081	9	20	22	6	4	0	14	12	0
$d_{xz} + d_{xz}$	126aβ	1.586	0	50	23	0	7	0	2	4	0
$d_{xy} - d_{xy}$	125aβ	1.461	13	29	20	18	6	0	0	0	0
$d_{xy} + d_{xy}$	124aβ	1.387	26	0	0	60	0	0	0	0	0
$d_{xz} - d_{xz}$	123aβ	1.304	4	48	2	35	0	0	0	0	0
$d_{yz} - d_{yz}$	122aβ	1.195	4	36	8	25	0	0	0	0	0
					Occupied						
π_x^*	131aα	0.657	0	0	6	0	12	0	37	21	0
π_y^*	130aα	0.216	0	0	0	0	1	0	32	55	0
π_y^*	121aβ	0.119	4	14	20	0	10	0	23	20	0
π_x^*	120aβ	−0.162	0	4	0	0	18	0	30	29	0

3. BS State. The BS calculation (Scheme 1, panel 1b, and lower panel of Table 1) represents a state similar, but not identical, to the antiferromagnetic state $|S_1S_2;0,0\rangle$. The orbital energy diagram for this state is given in Figure 5, and the compositions and energies of the highest occupied orbitals (the O_2 π^* orbitals) and of the lowest unoccupied orbitals (the dβ orbitals on Fe^1, same composition as dα orbitals of Fe^2) are shown in Table 3. Note that in the energy level diagram, the orbitals are arranged in columns according to their spatial distribution on the left and right of the molecule, and the columns for Fe^1, O_2, and Fe^2 are split in subcolumns according to the spin index.

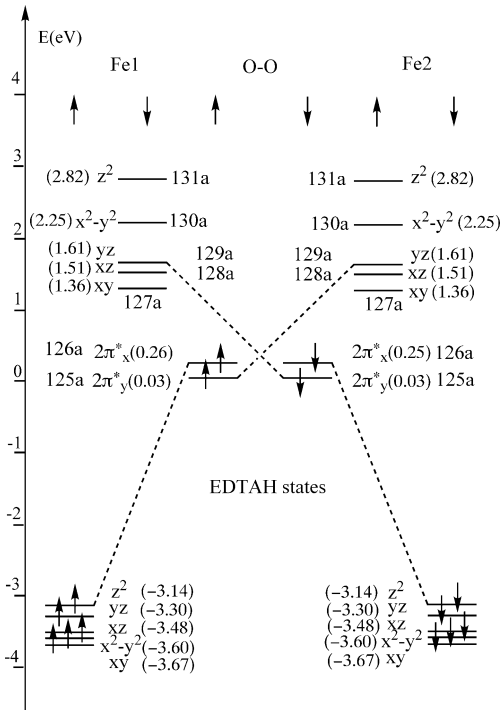

Figure 5. Orbital energy diagram for the BS calculation. Only orbitals with large Fe or O_2 character are shown. On Fe^1 (left) all the dα spin orbitals are occupied and strongly stabilized by the exchange interaction, the dβ orbitals are unoccupied and much higher in energy. On Fe^2 the role of dα and dβ orbitals is reversed. The π^* orbitals of O_2^{2-} are between the occupied/unoccupied d orbitals.

Due to the geometrical equivalence between the left and right halves of the homonuclear dimer, each spin-up level is energetically degenerate with a mirror image spin-down level. The orbitals can also be grouped in up-spin/down-spin pairs that have a large overlap of their spatial parts (the "same" orbitals), thus resembling doubly occupied orbitals in a closed shell system. However, these pairs are now nondegenerate, as a consequence of the spin polarization. This is particularly evident for the "mainly" Fe 3d orbitals, which show a huge energetic separation between spatially similar dα and dβ orbitals on one Fe. On Fe^1 there is a set of 5 low-lying occupied dα orbitals and a set of 5 high-lying unoccupied dβ orbitals. On Fe^2 the situation is reversed: low-lying occupied dβ orbitals and high-lying unoccupied dα orbitals. On O_2, the α and β π^* orbitals have equal energy. They establish similar interactions with the Fe ions, because of symmetry (see the typical interaction lines drawn in the figure), the role of the two Fe ions being reversed for the α and β partners. On the Fe ions there is also degeneracy between occupied α and β d orbitals, but in this case the orbitals in a degenerate pair are completely different, one being located on Fe^1, the other on Fe^2 or viceversa. On O_2, $\pi_a^*\alpha$ and $\pi_a^*\beta$ orbitals ($a = x$ or $a = y$) are also spatially inequivalent, because of different polarization from Fe^1 and Fe^2, but in this case the effect is small. These orbitals thus retain fully their π^* nature, although mixing is observed between their x and y components, see Table 3.

The magnitude of the interactions between the $Fe^{1,2}$ and O_2 are similar to those described above for the HS state. This fact is apparent from the orbital populations (Table 1, lower panel). In the BS state, by definition, Fe^1 carries 5 unpaired α d electrons, and Fe^2 5 β d electrons. The total amount of electronic charge donated to the empty d orbitals (1.14 electrons to each Fe) is practically the same as in the HS situation (1.12 electrons). Also, the charge donated by O_2^{2-} is analogous (remaining charge on O_2 is −0.68), as is the charge donated to the $Fe^{1,2}$ by the

TABLE 3: Energies (eV) and Composition (%) of the Unoccupied Spin-Down Orbitals Localised on Fe[1], and of the HOMO and HOMO-1 Spin-Down/Spin-Up Orbitals, for [(EDTAH)Fe(O$_2$)Fe(EDTAH)]$^{2-}$ at d(O−O) = 1.352 Å on S = 5 Spin Surface (BS)

BS, d(O−O) = 1.352 Å										
			Fe[1]					dioxygen		Fe[2]
level		energy	$d_{x^2-y^2}$	d_{xz}	d_{yz}	d_{xy}	d_{z^2}	π_x^*	π_y^*	
Unoccupied β Spin										
d_{z^2}	131aβ	2.818	7	0	18	0	42	7	5	0
$d_{x^2-y^2}$	130aβ	2.250	42	2	6	23	3	0	1	0
d_{yz}	129aβ	1.611	0	30	23	0	11	13	14	0
d_{xz}	128aβ	1.511	6	38	24	6	9	0	0	0
d_{xy}	127aβ	1.358	23	7	2	53	3	0	3	0
HOMO and HOMO-1 α and β Spin										
π_x^*	126aα	0.260	2	0	4	0	11	28	13	$5d_{z^2} + 2d_{yz}$
π_x^*	126aβ	0.254	0	0	2	0	5	28	13	$11d_{z^2} + 4d_{yz} + 2d_{x^2-y^2}$
π_y^*	125aα	0.033	0	0	0	0	2	21	41	$10d_{yz} + 8d_{z^2} + 6d_{xz} + 3d_{x^2-y^2}$
π_y^*	125aβ	0.029	3	6	10	0	8	21	41	$2d_{z^2}$

$EDTAH^{3-}$ ligands. The overall charges on $Fe^{1,2}$ are thus similar to the HS state (+1.09 electrons). The only difference between BS and HS states is in the α and β spin populations on O_2, which are equal by symmetry in BS, and intermediate between α and β π^* populations in HS. We therefore conclude that the BS state of [(EDTAH)Fe(O$_2$)Fe(EDTAH)]$^{2-}$ can be described satisfactorily as two HS Fe(III) S = 5/2 ions orbital-interacting with their negative $EDTAH^{3-}$ ligands (from which they receive a substantial amount of electron charge), and exchange-coupled through the O_2^{2-} group.

4. O−O Cleavage Reaction. We have calculated the Heisenberg J constant as a function of the O−O distance by performing both HS and BS calculations at a number of points along the O−O bond breaking coordinate, cf. ref 51. At each point, the O−O distance was constrained and all other geometric degrees of freedom were optimized. Results for the HS ($S = S_{max} = 5$) and $S = S_{min} = 0$ energy dependences on d(O−O) are shown in Figure 6. We notice that the BS state is always more stable than the HS S = 5 state, which means that antiferromagnetic coupling (S = 0) between the Fe(III) ions is favored throughout the O−O dissociation on this energy surface. A value of J = −55 cm^{-1} was computed for the initial [(EDTAH)Fe(O$_2$)Fe(EDTAH)]$^{2-}$ complex, which agrees in sign and magnitude to values calculated for model systems for biological nonheme dinuclear iron active sites.[31,84–86] Negative and small values of J (−18/−101 cm^{-1}) were calculated along the reaction path, indicating weak antiferromagnetic coupling between the $S_1 = S_2$ = 5/2 Fe centers along the whole reaction pathway. The most important observation, however, is that the ferromagnetic and antiferromagnetic states follow almost parallel curves and they both exhibit a high transition-state barrier for O−O breaking. Indeed, the O−O cleavage process *cannot* be eased by coupling the HS Fe ions to form any of the other states belonging to the Heisenberg ladder. Therefore the exchange-coupling interaction appears to be irrelevant for the chemistry of the O−O cleavage.

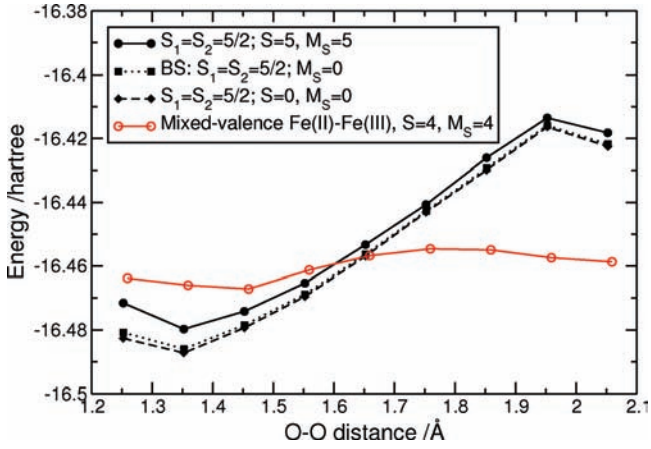

Figure 6. Energy curves along the O−O distance coordinate (all other geometry parameters optimized). In addition to the curve for the ferromagnetic $S = S_{max} = 5$ HS electron configuration of two S = 2.5 Fe centers (cf. Figure 14 of ref 51), the corresponding BS state, as well as the antiferromagnetic $S = S_{min} = 0$ state deduced from them are given. Also the S = 4 energy curve for a different electron configuration (see text) is shown (red).

It is not difficult to see why this is the case. The various states of the Heisenberg ladder only differ, at the orbital level, in the spin occupations of the d orbitals of the two Fe centers. There always remain 5 d electrons on each Fe, and the situation for the O_2 fragment is bound to vary only between the lowest and highest "pegs" of the Heisenberg ladder, namely the HS and S = 0 (close to BS) states. The O−O bond is insensitive to the exchange coupling, although the Fe−O_2 bond will be somewhat affected by the different d spin orbital occupations in the different states of the Heisenberg ladder. We have already observed that there is little difference between the O_2 moieties in the HS and BS cases. Thus the basic approximation of the BS-DFT approach, weak exchange coupling through a ligand bridging two magnetic centers, is supported, indirectly, by our analysis.

As noted in ref 51, an increase in the O−O distance in [(EDTAH)Fe(O$_2$)Fe(EDTAH)]$^{2-}$ brings about a progressive stabilization of a state of lower spin multiplicity (S = 4). This is not a state of the Heisenberg ladder, but it is generated by excitation of one electron from the highest α spin orbital (131a-$\pi^*\alpha$ in the HS state of Figure 4) to the lowest empty β spin orbital (122a-$d_{xz}\beta$). The resulting MO energies are displayed in Figure 7. It is clear that in this case a real change of electron configuration has occurred, which is the crucial factor affecting the behavior of this state in the O−O bond breaking process. Here, one electron is transferred from O_2^{2-} to Fe, and the electronic configuration evolves from two S = 5/2 high-spin Fe(III) ions, coupled through the peroxo O_2^{2-} bridge, to a mixed valence (MV) Fe(II)−Fe(III) pair of ions, coupled through a superoxo O_2^- bridge. The HS S = 4 calculation represented in Figure 7 describes the symmetrical combination of the Fe^1(II)−Fe^2(III) and Fe^1(III)−Fe^2(II) situations.

The configuration change to the MV compound promotes the O−O bond breaking process. At a distance of ∼1.6 Å, the

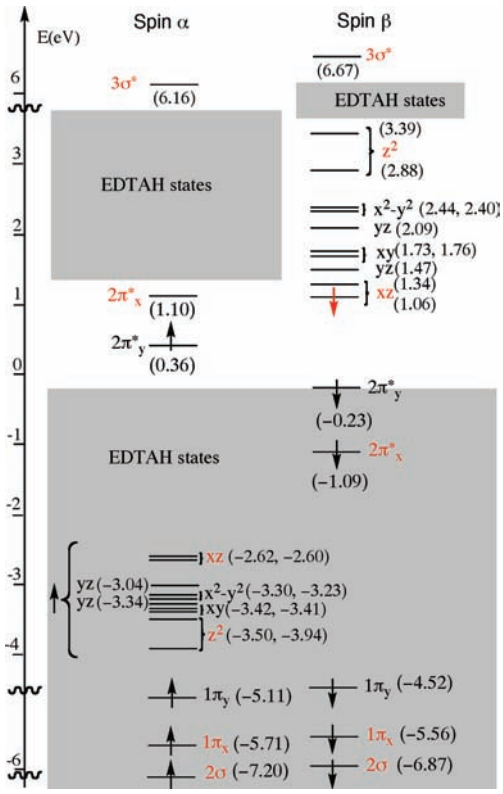

Figure 7. Orbital energy diagram for the $S = 4$ electron configuration, where the red electron has been transferred from the O_2 $2\pi^*_x\alpha$ orbital to the $(d_{xz} - d_{xz})\beta$ orbital, forming a formally superoxo (O_2^-) ion and a (symmetrized) mixed valence pair Fe(II)−Fe(III).

energies of the $S = 5$ and $S = 4$ states are comparable, and after this point the latter becomes more stable. The transition state for the bond cleavage (∼1.75 Å) is on the $S = 4$ surface, which, after the bond cleavage is complete, leads to two high spin ($S_1 = S_2 = 2$) [EDTAH.FeO]$^-$ units, which are ferromagnetically coupled ($S = S_1 + S_2 = 4$). Such HS ($S = 2$) FeO^{2+} units in a suitable ligand environment have been shown to be highly active oxidants for organic substrates (see ref 61 for the influence of the $EDTAH_n^{-4+n}$ ligands on the FeO^{2+} reactivity).

Interestingly, constraining the O−O cleavage to proceed on the $S = 5$ energy surface leads to the dissociation of [(EDTAH)Fe(O_2)Fe(EDTAH)]$^{2-}$ into two nonequivalent moieties, with the O−O group rearranging to side-on (η^2) coordination to one Fe center, and coordinating more loosely to the second one (see Figure 3). The activation energy for the O−O cleavage, computed as the energy difference between the $S = 4$ transition state and the initial $S = 0$ [(EDTAH)Fe(O_2)Fe(EDTAH)]$^{2-}$ complex amounts to 85.6 kJ mol^{-1} (to be compared to a value of ∼77 kJ mol^{-1}, as estimated in ref 51 with respect to the initial $S = 5$ state). In order to understand this reaction we need to analyze why the single spin-flip excitation from the $S = 5$ to the $S = 4$ surface, which is a transition to the mixed valence configuration, makes such an important difference, both for the height of the transition barrier and for the nature of the products. We will analyze this issue in the next section.

B. Electronic Structure Analysis of the O−O Bond Breaking Process on the $S = 4$ Surface. The O−O bond breaking leads to a product which consists of two FeO^{2+} units enclosed in an $EDTAH^{3-}$ ligand cage, with the two [EDTAH.FeO]$^-$ complexes being held together by two hydrogen bonds, see Figure 2. Our structure is more asymmetric (two Fe−O bonds are much shorter than the other two) than the models for

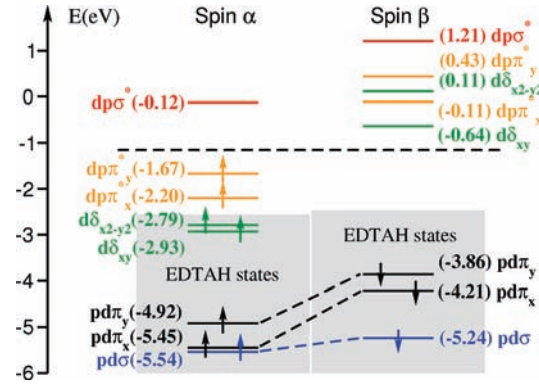

Figure 8. Orbital energy diagram for the [EDTAH·FeO]$^-$ complex. The σ and π Fe−O bonding orbitals (formally O p, here denoted pdσ and pdπ) are blue, the dδ orbitals $d_{x^2-y^2}$ and d_{xy} green and the π antibonding orbitals (formally d, here denoted dpπ*) orange. The important σ antibonding orbital (formally d_{z^2}, here denoted dpσ*) is in red.

compound Q of MMO in the literature.[31,85,86] The electronic structure of various $[EDTAH_n^{-4+n}.FeO^{2+}]^{-2+n}$ complexes has been discussed in detail in ref 61. We show the orbital energy diagram of the ferryl complex [EDTAH.FeO]$^-$ in Figure 8, which is analogous to the one of the pentaaqua complex, $(H_2O)_5FeO^{2+}$.[22,63] The FeO^{2+} orbitals resemble O_2 orbitals, except that the Fe d_σ (d_{z^2}) and d_π (d_{xz} and d_{yz}) orbitals replace one set of O p_σ and p_π orbitals in the formation of σ and π bonds. At the bottom of the level diagram we find the $d_\sigma + p_\sigma \equiv$ pdσ and $d_\pi + p_\pi \equiv$ pdπ orbitals that form the σ and π bonds. Both the α and β spin components of these bonding orbitals are occupied. As in O_2 there are two unpaired spins in the $\pi^*\alpha$ antibonding orbitals, which in this case are d−p π antibonding orbitals; we denote them dpπ*. The dδ orbitals ($d_{x^2-y^2}$ and d_{xy}) are nonbonding with respect to the Fe−O bond; they do of course interact with the equatorial O and N atoms of the $EDTAH^{3-}$ ligand, which accounts for the splitting between the two dδ levels. This splitting is much smaller than in the case of equatorial water ligands, see ref 62. For the dδ orbitals, the α ones, $d_{xy}\alpha$ and $d_{x^2-y^2}\alpha$, are occupied, but their β counterparts are unoccupied. Together with the two unpaired spins in the dp$\pi^*\alpha$ orbitals, they give four unpaired α spins. The resulting considerable exchange stabilization of the α spin orbitals with respect to the β ones, in particular the stabilization of the lowest unoccupied α spin orbital (dp$\sigma^*\alpha$), is the primary factor in promoting the aptitude of this orbital to accept electrons from a substrate.[26,62,63] Furthermore, dpσ* is the antibonding partner of the $d_{z^2} - p_z$ orbital, and it has considerable amplitude outside the O(oxo) atom. Although in a ligand-field context pdσ would be regarded as an "oxygen lone pair" and the dpσ* as the "d_{z^2}" orbital, these orbitals are mixtures of the O2p_z and d_{z^2} AOs with comparable weights (i.e., the bond is rather covalent). The dpσ*, corresponding nominally to the d_{z^2} orbital, has in fact a higher oxygen character (48% in bare FeO^{2+}) than d_{z^2} character (37%), see ref 22, which explains its large amplitude at the O end of the oxo group.

After the O−O bond breaking, when the two [EDTAH.FeO]$^-$ monomers are only loosely coupled via H bonds, we expect the symmetric and antisymmetric combinations of the orbitals of Figure 8 to appear clearly in the MO diagram of the complex. Indeed, these combinations can be easily identified in Figure 9. These orbitals are embedded in a large number of $EDTAH^{3-}$-based orbitals, indicated with a gray background in the figure. In the virtual spectrum, among the spin α levels the + and − combinations of the catalytically crucial acceptor orbital dp $\sigma^*\alpha$

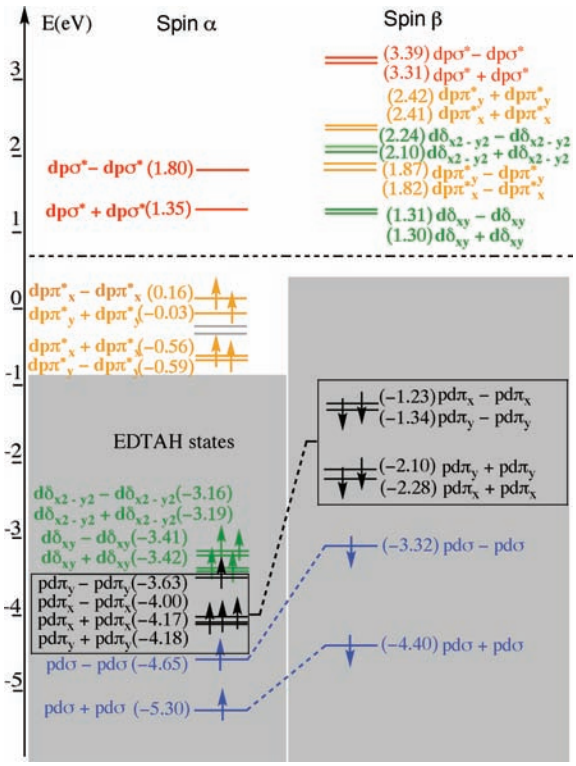

Figure 9. Orbital level diagram of the product on the $S = 4$ surface, with dissociated O−O bond, see Figure 2. The same color coding as in Figure 8 is applied.

are also easily identified. Their splitting is considerable (0.45 eV), since their large amplitudes along the Fe−O axis promotes orbital mixing, even at relatively large distances. An even larger splitting is observed between the + and − combinations of the bonding pdσ orbitals, which are at the bottom of the level diagram of Figure 9. The orbitals that are perpendicular to the Fe−O axis, such as the bonding pd$\pi_{x,y}$ and the antibonding dp$\pi^*_{x,y}$ orbitals show only a moderate energy split, which is further reduced for the dδ orbitals. After the breaking of the two hydrogen bonds in the $[(EDTAH)FeO\cdots OFe(EDTAH)]^{2-}$ complex, a process likely to occur in aqueous solution at room temperature and pressure, the two $[EDTAH.FeO]^-$ complexes can potentially act as strong oxidants, because of the presence in their spectrum of the low-lying dp $\sigma^*\alpha$ orbitals newly generated by the O_2 cleavage.

It remains now to be explained why the change from HS to MV configuration (associated with the $S = 5 \rightarrow S = 4$ spin transition) described in section IIIA4 is beneficial for the O−O bond breaking process. At first sight this may seem unexpected, since there are fewer antibonding electrons on O_2 in O_2^- than in O_2^{2-}. In Scheme 2 we show energy levels from orbitals involved in the HS → MV transition and in the O−O bond breaking. On the left are orbitals of the "reactant" (the [EDTAH.Fe(III)-O_2-Fe(III).EDTAH] complex), cf. Figure 1, on the right those of the product, the $[EDTAH.Fe(IV)O\cdots OFe(IV).EDTAH]^{2-}$ dimer, cf. Figure 2. We consider in Scheme 2 the orbitals with lobes in the xz plane. The $\pi^*_y\alpha$ and $\pi^*_y\beta$ orbitals perpendicular to this plane, which are both occupied initially (see Figure 7), will be considered later.

In Scheme 2 (left) the "in-plane" orbitals 2σ, $1\pi_x$, $2\pi^*_x$, and $3\sigma^*$ of O_2 are shown together with the in-plane d orbitals with which they interact, the d_{xz} and d_{z^2} combinations of the dinuclear Fe−Fe core. The occupations and the connections between the reactant and the product levels are drawn in Scheme 3 for the

SCHEME 2: Left: In-Plane (xz Plane) Orbitals of the Reactant [EDTAH·Fe(III)-O_2-Fe(III)·EDTAH] Complex, cf. Figure 1 and Right: Corresponding Orbitals of the Product $[EDTAH\cdot Fe(IV)O\text{-}OFe(IV)\cdot EDTAH]^{2-}$ Dimer, cf. Figure 2

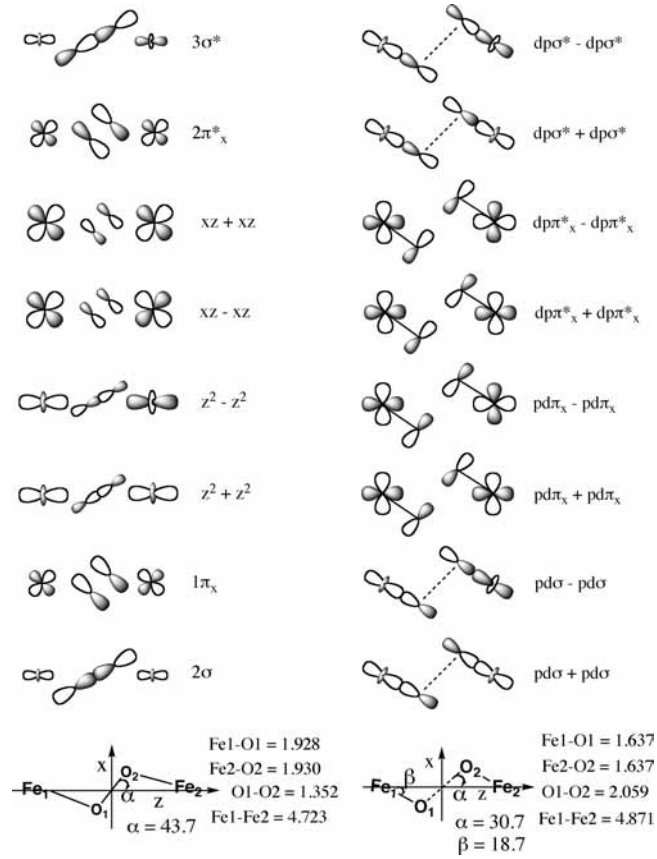

SCHEME 3: Left: MO Diagram for the α Spin Orbitals of the Reactant [EDTAH·Fe(III)-O_2-Fe(III)·EDTAH] and Right: Corresponding Orbitals of the Product [EDTAH·FeO−OFe·EDTAH] Dimer

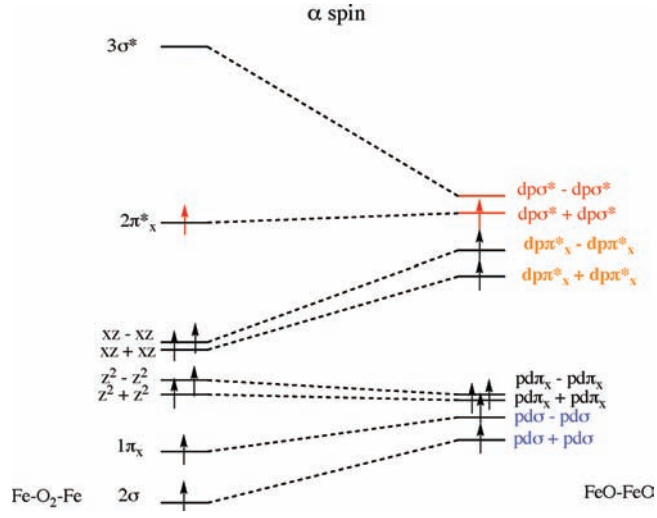

α spin manifold. The crucial change in the electronic configuration at the HS → MV transition is the promotion of a spin α electron (in red) from the π^*_x orbital in Scheme 3 to the β spin $d_{xz} - d_{xz}$ orbital (Scheme 4). If, by contrast, the reaction were bound to take place on the $S = 5$ surface, the electron would end up in the lowest of the two combinations of dpσ^*

SCHEME 4: Left: MO Diagram for the β Spin Orbitals of the Reactant [EDTAH·Fe(III)-O_2-Fe(III)·EDTAH] and Right: Corresponding Orbitals of the Product [EDTAH·FeO−OFe·EDTAH] Dimer

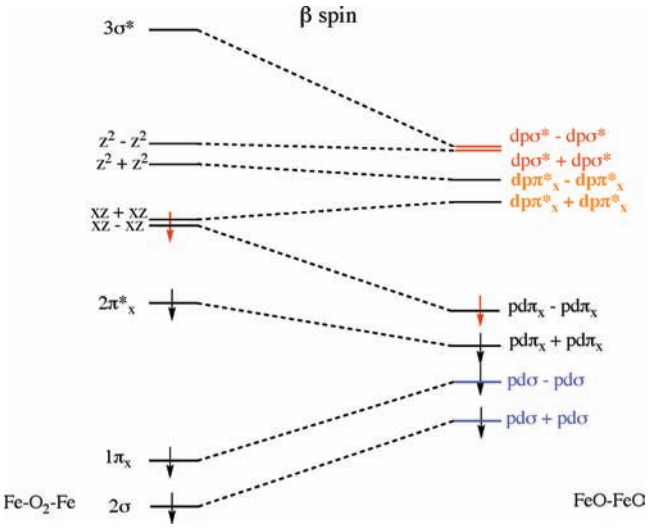

orbitals, dpσ* + dpσ* in Scheme 3. This implies that the reaction would proceed in that case to an excited state. Upon separation of the two monomers, the electron would end up in the dpσ* orbital of one of the [EDTAH·FeO]$^-$ monomers. This is detrimental for the action of this moiety as an oxidative agent, since the occupied dpσ* orbital can no longer act as acceptor orbital. But the important point for an understanding of the lower barrier on the $S = 4$ surface, is of course that after transfer of the electron to the $(d_{xz} - d_{xz})\beta$ orbital, the reaction can proceed to the ground state. The transferred electron ends up, in Scheme 4, in a combination of the low-lying bonding pdπ_x orbitals of the FeO unit. Clearly, the $(d_{xz} - d_{xz})\beta$ orbital experiences a substantial stabilization in the course of the reaction while transforming into the bonding $(pd\pi_x - pd\pi_x)\beta$ orbital. At −1.23 eV, this is much lower in energy than the $(d_{xz} - d_{xz})\beta$ orbital (1.06 eV) from which it develops during O−O stretching, and even than the $2\pi_x^*\alpha$ orbital which the electron was initially occupying (0.66 eV).

In summary, the reaction on the $S = 5$ surface ends up in a $pd\pi_x \rightarrow dp\sigma^*$ excited state, while the $\pi_x^* \rightarrow (d_{xz} - d_{xz})\beta$ excitation allows the reaction to proceed to the product ground state. The O−O cleavage process in [(EDTAH)Fe(O_2)-Fe(EDTAH)]$^{2-}$ can therefore be described as a symmetry forbidden reaction on the $S = 5$ surface that becomes symmetry allowed by excitation of the $2\pi_x^*\alpha$ electron to $(d_{xz} - d_{xz})\beta$, with the consequent involvement of the lower multiplicity $S = 4$ state. ("Symmetry" here obviously refers to spin symmetry).

For completeness we also briefly describe the situation for the out-of-plane orbitals. The α orbitals to be considered are, for the reactant, in energetic order, the bonding O_2 $1\pi_y$, the metal-ion $d_{yz} + d_{yz}$ and $d_{yz} - d_{yz}$, and the antibonding O_2 $2\pi_y^*$, see Figure 7. All of them are occupied. At the product side, the following α spin orbitals, also occupied, appear in increasing energy order: $pd\pi_y + pd\pi_y$, $pd\pi_y - pd\pi_y$, $dp\pi_y^* + dp\pi_y^*$, and $dp\pi_y^* - dp\pi_y^*$, see Figure 9. Having all relevant orbitals occupied with one α spin electron in both reactant and product, the reactant α out-of-plane orbitals can evolve to the product orbitals without changes in electronic configuration. For the β spin we need to consider the same spatial orbitals for the reactant: $1\pi_y$, $2\pi_y^*$, $d_{yz} + d_{yz}$, and $d_{yz} - d_{yz}$ (Figure 7). Now only the two lowest orbitals are occupied. In the product, these orbitals give rise to the same orbitals as in the α case, $pd\pi_y + pd\pi_y$, $pd\pi_y - pd\pi_y$, $dp\pi_y^* + dp\pi_y^*$, and $dp\pi_y^* - dp\pi_y^*$ (Figure 9). Since in this case the high-lying "d" orbitals $dp\pi_y^* + dp\pi_y^*$ and $dp\pi_y^* - dp\pi_y^*$ are empty, the two β electrons of the reactant in the O_2 π_y and π_y^* orbitals can be promoted to the two low-lying $pd\pi_y + pd\pi_y$ and $pd\pi_y - pd\pi_y$ orbitals. We conclude that for the out-of-plane orbitals there is no orbital-symmetry restriction in either the α or β spin manifolds.

IV. Summary and Conclusions

We have examined the electronic structure of the gas phase [(EDTAH)Fe(O_2)Fe(EDTAH)]$^{2-}$ complex, the hypothetical dinuclear intermediate appearing in the multistep mechanism for the Fe(II)-to-Fe(III) autoxidation reaction proposed by van Eldik and co-workers on the basis of kinetic measurements. The O_2 molecule in this system is formally reduced to a peroxide ion (as assumed in refs.[53–55]), and it mediates the coupling between the two remote (∼4.72 Å) magnetic ions via superexchange. We have addressed the issue of the magnetic coupling between the two spin polarized metal ion centers, using BS DFT calculations. Our results support the finding of ref 51, according to which the complex in its optimized geometry resides on the $S = 5$ spin surface. We have found that there is antiferromagnetic coupling between the two magnetic centers, yielding an $S = 0$ lowest state which is 19.7 kJ mol^{-1} lower than the ferromagnetically coupled state $S = 5$. Heisenberg coupling constants computed for the $S = 5$ state are in agreement with values computed for biological model compounds.[31,84–86] However, we find computationally, and have rationalized by electronic structure considerations, that exchange coupling is of little relevance for the O−O bond breaking. The different spin couplings leading to the Heisenberg ladder of spin states do not make much difference for the O−O bond, and the barrier to dissociation is basically the same and rather high (186.0 kJ mol^{-1}) for all those states. In fact, if the reaction is constrained to take place on the $S = 5$ (or $S = 0$) surface with two $S = 5/2$ Fe centers, either ferromagnetically or antiferromagnetically coupled, the dinuclear complex decomposes into two inequivalent systems, with an O_2 molecule (or two oxo groups) coordinated to only one metal center, similar to the situation observed in several metallo-organic O_2 adducts (see, e.g., ref 87).

When O−O cleavage is induced by progressive increase in the O−O distance, we find, consistent with ref 51, that the complex can lower the reaction barrier by undergoing a transition to an $S = 4$ state as the O−O distance increases. We have shown that this change of spin state involves a transition to an Fe(II)−Fe(III) mixed valence complex. The O−O cleavage barrier is in this case much lower, since the reaction, which was symmetry forbidden on the $S = 5$ surface, is symmetry allowed in the electronic configuration of the $S = 4$ state. The final product consists of two [FeO.EDTAH]$^-$ complexes, both in a quintet ground state $S = 2$, which are held together by two hydrogen bonds between the [EDTAH]$^{3-}$ ligands of the two Fe ions. These ferryl complexes are then in the spin state which is the most favorable for oxidation activity. Besides, [EDTAH]$^{3-}$ provides an ideal ligand environment for further promoting the catalytic activity of the FeO^{2+} group.[61]

The reaction barrier for the O−O cleavage on the $S = 4$ surface (85.6 kJ mol^{-1}) is close to values estimated from models of active centers of O_2 activating metallo-enzymes. Our product has a structure resembling the Fe−O_2−Fe diamond structure often attributed to compound **Q** of MMO or compound **X** of ribonucleotide reductase, which have been extensively studied

computationally.[3,29,31,60,84–86,88–91] However the difference between the two types of Fe−O bonds is much larger than has been found for compound **Q**; we have arrived at two true Fe(IV)oxo groups, with characteristic short Fe−O bonds. It is a matter for future investigation whether the configuration change we have found to play a key role in enabling this reaction product could also play a role in the biological systems. The influence of solvation on the energetics of the O−O activation in Fe(II)/EDTA complexes in water will also be treated in detail in a future publication. Our results certainly support the hypothesis that O−O activation and cleavage in $[(EDTAH)Fe(O_2)\text{-}Fe(EDTAH)]^{2-}$ may be induced in abiotic experimental conditions, leading to the generation of highly reactive high spin ferryl complexes.

Acknowledgment. This work was funded by the National Research School Combination "Catalysis by Design. P.B. carried out this work under the HPC-EUROPA project (RII3-CT-2003-506079), with the support of the European Community-Research Infrastructure Action under the FP6 "Structuring the European Research Area" Programme.

References and Notes

(1) Babcock, G. T. *Proc. Natl. Acad. Sci. U.S.A.* **1999**, *96*, 12971–12973.
(2) Groves, J. T. *J. Inorg. Biochem.* **2006**, *100*, 434–447.
(3) Bassan, A.; Blomberg, M. R. A.; Borowski, T.; Siegbahn, P. E. M. *J. Inorg. Biochem.* **2006**, *100*, 727–743.
(4) Debrunner, P. G. *Hyperfine Interact.* **1990**, *53*, 21–36.
(5) Rutter, R.; Valentine, M.; Hendrich, M. P.; Hager, L. P.; Debrunner, P. G. *Biochemistry* **1983**, *22*, 4769–4774.
(6) Rutter, R.; Hager, L. P.; Dhonau, H.; Hendrich, M.; Valentine, M.; Debrunner, P. *Biochemistry* **1984**, *23*, 6809–6816.
(7) Schulz, C. E.; Devaney, P. W.; Winkler, H.; Debrunner, P. G.; Doan, N.; Chiang, R.; Rutter, R.; Hager, L. P. *FEBS Lett.* **1979**, *103*, 102–105.
(8) Schulz, C. E.; Rutter, R.; Sage, J. T.; Debrunner, P. G.; Hager, L. P. *Biochemistry* **1984**, *23*, 4743–4754.
(9) Hersleth, H.-P.; Ryde, U.; Rydberg, P.; Görbitz, C. H.; Andersson, K. K. *J. Inorg. Biochem.* **2006**, *100*, 460–476.
(10) Price, J. C.; Barr, E. W.; Tirupati, B.; Bollinger, J. M., Jr.; Krebs, C. *Biochemistry* **2003**, *42*, 7497–7508.
(11) Price, J. C.; Barr, E. W.; Glass, T. E.; Krebs, C.; Bollinger, J. M., Jr. *J. Am. Chem. Soc.* **2003**, *125*, 13008–13009.
(12) Proshlyakov, D. A.; Henshaw, T. F.; Monterosso, G. R.; Ryle, M. J.; Hausinger, R. P. *J. Am. Chem. Soc.* **2004**, *126*, 1022–1023.
(13) Kryatov, S. V.; Rybak-Akimova, E. V.; Schindler, S. *Chem. Rev.* **2005**, *105*, 2175–2226.
(14) Solomon, E. I.; Brunold, T. C.; Davis, M. I.; Kemsley, J. N.; Lee, S.-K.; Lehnert, N.; Neese, F.; Skulan, A. J.; Yang, Y.-S.; Zhou, J. *Chem. Rev.* **2000**, *100*, 235–349.
(15) Kaizer, J.; Klinker, E. J.; Oh, N. Y.; Rohde, J.-U.; Song, W. J.; Stubna, A.; Kim, J.; Münck, E.; Nam, W.; Que, L., Jr. *J. Am. Chem. Soc.* **2003**, *126*, 472–473.
(16) Price, J. C.; Barr, E. W.; Glass, T. E.; Krebs, C.; Bollinger, J. M., Jr. *J. Am. Chem. Soc.* **2003**, *125*, 13008–13009.
(17) Shaik, S.; Filatov, M.; Schröder, D.; Schwarz, H. *Chem.—Eur. J.* **1998**, *4*, 193–199.
(18) Harris, N.; Shaik, S.; Schröder, D.; Schwarz, H. *Helv. Chim. Acta* **1999**, *82*, 1784–1797.
(19) Schröder, D.; Shaik, S.; Schwarz, H. *Acc. Chem. Res.* **2000**, *33*, 139–145.
(20) Buda, F.; Ensing, B.; Gribnau, M. C. M.; Baerends, E. J. *Chem.—Eur. J.* **2001**, *7*, 2775–2783.
(21) Bassan, A.; Blomberg, M. R. A.; Siegbahn, P. E. M. *Chem.—Eur. J.* **2003**, *9*, 106–115.
(22) Buda, F.; Ensing, B.; Gribnau, M. C. M.; Baerends, E. J. *Chem.—Eur. J.* **2003**, *9*, 3436–3444.
(23) Decker, A.; Rohde, J.-U.; Que, Jr, L.; Solomon, E. I. *J. Am. Chem. Soc.* **2004**, *126*, 5378–5379.
(24) Ghosh, A.; Tangen, E.; Ryeng, H.; Taylor, P. R. *Eur. J. Inorg. Chem.* **2004**, *23*, 4555–4560.
(25) Schöneboom, J. C.; Neese, F.; Thiel, W. *J. Am. Chem. Soc.* **2005**, *127*, 5840–5853.
(26) Decker, A.; Clay, M. D.; Solomon, E. I. *J. Inorg. Biochem.* **2006**, *100*, 697–706.
(27) Neese, F. *J. Inorg. Biochem.* **2006**, *100*, 716–726.
(28) Yoshizawa, K. *Acc. Chem. Res.* **2006**, *39*, 375–382.
(29) Siegbahn, P. E. M.; Crabtree, R. H.; Nordlund, P. *J. Biol. Inorg. Chem.* **1998**, *3*, 314–317.
(30) Lieberman, R. L.; Rosenzweig, A. C. *Nature* **2005**, *34*, 177–182.
(31) Siegbahn, P. E. M. *Inorg. Chem.* **1999**, *38*, 2880–2889.
(32) Lind, T.; Siegbahn, P. E. M.; Crabtree, R. H. *J. Phys. Chem. B* **1999**, *103*, 1193–1202.
(33) Groves, J. T.; Van Der Puy, M. *J. Am. Chem. Soc.* **1974**, *96*, 5274–5275.
(34) Groves, J. T.; McClusky, G. A. *J. Am. Chem. Soc.* **1976**, *98*, 859–861.
(35) Guallar, V.; Friesner, R. A. *J. Am. Chem. Soc.* **2004**, *126*, 8501–8508.
(36) Altun, A.; Guallar, V.; Friesner, R. A.; Shaik, S.; Thiel, W. *J. Am. Chem. Soc.* **2006**, *128*, 3924–3925.
(37) Løgager, T.; Holcman, J.; Sehested, K.; Pedersen, T. *Inorg. Chem.* **1992**, *31*, 3523–3529.
(38) Pestovsky, O.; Bakac, A. *J. Am. Chem. Soc.* **2004**, *126*, 13757–13764.
(39) Pestovsky, O.; Stoian, S.; Bominaar, E. L.; Shan, X.; Münck, E.; Que, Jr, L.; Bakac, A. *Angew. Chem., Int. Ed.* **2005**, *44*, 6871–6874.
(40) Ensing, B.; Buda, F.; Blöchl, P.; Baerends, E. J. *Angew. Chem., Int. Ed.* **2001**, *40*, 2893–2895.
(41) Ensing, B.; Buda, F.; Blöchl, P.; Baerends, E. J. *Phys. Chem. Chem. Phys.* **2002**, *4*, 3619–3627.
(42) Ensing, B.; Buda, F.; Gribnau, M. C. M.; Baerends, E. J. *J. Am. Chem. Soc.* **2004**, *126*, 4355–4365.
(43) Bray, W. C.; Gorin, M. H. *J. Am. Chem. Soc.* **1932**, *54*, 2124–2125.
(44) Wardman, P.; Candeias, L. P. *Radiat. Res.* **1996**, *145*, 523–531.
(45) Dunford, H. B. *Coord. Chem. Rev.* **2002**, *233*, 311–318.
(46) Gozzo, F. *J. Mol. Catal. A: Chem.* **2001**, *171*, 1–22.
(47) Englehardt, J. D.; Meeroff, D. E.; Echegoyen, L.; Deng, Y.; Raymo, F. M.; Shibata, T. *Environ. Sci. Technol.* **2007**, *41*, 270–276.
(48) Noradoun, C. E.; Cheng, I. F. *Environ. Sci. Technol.* **2005**, *39*, 7158–7163.
(49) Welch, K. D.; Davis, T. Z.; Aust, S. D. *Arch. Biochem. Biophys.* **2002**, *397*, 360–369.
(50) Gambardella, F.; Ganzeveld, I. J.; Winkelman, J. G. M.; Heeres, E. J. *Ind. Eng. Chem. Res.* **2005**, *44*, 8190–8198.
(51) Bernasconi, L.; Baerends, E. J. *Inorg. Chem.* **2009**, *48*, 527–540.
(52) Zang, V.; van Eldik, R. *Inorg. Chem.* **1990**, *29*, 1705–1711.
(53) Seibig, S.; van Eldik, R. *Inorg. Chem.* **1997**, *36*, 4115–4120.
(54) Seibig, S.; van Eldik, R. *Eur. J. Inorg. Chem.* **1999**, *1999*, 447–454.
(55) Seibig, S.; van Eldik, R. *Inorg. React. Mech.* **1999**, *1*, 91–105.
(56) Bukowski, M. R.; Koehntop, K. D.; Stubna, A.; Bominaar, E. L.; Halfen, J. A.; Münck, E.; Nam, W.; Que, L., Jr. *Science* **2005**, *310*, 1000–1002.
(57) Rohde, J.-U.; Que, L., Jr. *Angew. Chem., Int. Ed.* **2005**, *44*, 2255–2258.
(58) Rohde, J.-U.; In, J.-H.; Lim, M. H.; Brennessel, W. W.; Bukowski, M. R.; Stubna, A.; Münck, E.; Nam, W.; Que, L., Jr. *Science* **2003**, *299*, 1037–1039.
(59) Sastri, C. V.; Park, M. J.; Ohta, T.; Jackson, T. A.; Stubna, A.; Seo, M. S.; Lee, J.; Kim, J.; Kitagawa, T.; Münck, E.; Que, L., Jr.; Nam, W. *J. Am. Chem. Soc.* **2005**, *127*, 12494–12495.
(60) Shan, X.; Que, L., Jr. *J. Inorg. Biochem.* **2006**, *100*, 421–433.
(61) Bernasconi, L.; Baerends, E. J. *Eur. J. Inorg. Chem.* **2008**, *2008*, 1672–1681.
(62) Bernasconi, L.; Louwerse, M. J.; Baerends, E. J. *Eur. J. Inorg. Chem.* **2007**, *2007*, 3023–3033.
(63) Louwerse, M. J.; Baerends, E. J. *Phys. Chem. Chem. Phys.* **2007**, *9*, 156–166.
(64) Noodleman, L.; Norman, J. G. *J. Chem. Phys.* **1979**, *70*, 4903–4906.
(65) Noodleman, L. *J. Chem. Phys.* **1981**, *74*, 5737–5743.
(66) Noodleman, L.; Case, D. A.; Aizman, A. *J. Am. Chem. Soc.* **1988**, *110*, 1001–1005.
(67) Noodleman, L.; Davidson, E. R. *Chem. Phys.* **1986**, *109*, 131−143.
(68) Noodleman, L.; Case, D. A. In *Advances in Inorganic Chemistry*; Cammack, R., Ed.; Academic Press: New York, 1992; Vol. 38, pp 423−470 and references cited therein.
(69) Lovell, T.; Li, J.; Noodleman, L. *Inorg. Chem.* **2001**, *40*, 5251–5266.
(70) Noodleman, L.; Baerends, E. J. *J. Am. Chem. Soc.* **1984**, *106*, 2316–2327.
(71) Norman, J. C., Jr.; Ryan, P. B.; Noodleman, L. *J. Am. Chem. Soc.* **1980**, *102*, 4279–4282.
(72) Aizman, A.; Case, D. A. *J. Am. Chem. Soc.* **1982**, *104*, 3269–3279.
(73) Belanzoni, P.; Re, N.; Sgamellotti, A.; Baerends, E. J.; Floriani, C. *Inorg. Chem.* **1996**, *35*, 7776–7785.

(74) ADF2007.01, SCM, *Theoretical Chemistry*, Vrije Universiteit Amsterdam, The Netherlands, 2007; http://www.scm.com.
(75) Baerends, E. J.; Ellis, D. E.; Ros, P. *Chem. Phys.* **1973**, *2*, 41–51.
(76) Fonseca Guerra, C.; Snijders, J. G.; te Velde, G.; Baerends, E. J. *Theor. Chem. Acc.* **1998**, *99*, 391–403.
(77) van Lenthe, E.; Baerends, E. J.; Snijders, J. G. *J. Chem. Phys.* **1994**, *101*, 9783–9792.
(78) van Lenthe, E.; van Leeuwen, R.; Baerends, E. J.; Snijders, J. G. *Int. J. Quantum Chem.* **1996**, *57*, 281–293.
(79) Handy, N. C.; Cohen, A. J. *Mol. Phys.* **2001**, *99*, 403–412.
(80) Perdew, J. P.; Burke, K.; Ernzerhof, M. *Phys. Rev. Lett.* **1996**, *77*, 3865–3868.
(81) Swart, M.; Groenhof, A. R.; Ehlers, A. W.; Lammertsma, K. *J. Phys. Chem. A* **2004**, *108*, 5479–5483.
(82) Fouqueau, A.; Mer, S.; Casida, M. E.; Daku, L. M. L.; Hauser, A.; Mineva, T.; Neese, F. *J. Chem. Phys.* **2004**, *120*, 9473–9486.
(83) Fouqueau, A.; Casida, M. E.; Daku, L. M. L.; Hauser, A.; Neese, F. *J. Chem. Phys.* **2005**, *122*, 044110.
(84) Brunold, T. C.; Tamura, N.; Kitajima, N.; Moro-Oka, Y.; Solomon, E. I. *J. Am. Chem. Soc.* **1998**, *120*, 5674–5690.
(85) Baik, M.-H.; Gherman, B. F.; Friesner, R. A.; Lippard, S. J. *J. Am. Chem. Soc.* **2002**, *124*, 14508–14515.
(86) Gherman, B. F.; Baik, M. H.; Lippard, S. J.; Friesner, R. A. *J. Am. Chem. Soc.* **2004**, *126*, 2978–2990.
(87) Cramer, C. J.; Tolman, W. B.; Theopold, K. H.; Rheingold, A. L. *Proc. Natl. Acad. Sci. U.S.A.* **2003**, *100*, 3635–3640.
(88) Siegbahn, P. E. M.; Crabtree, R. H. *J. Am. Chem. Soc.* **1997**, *119*, 3103–3113.
(89) Han, W. G.; Liu, T. Q.; Lovell, T.; Noodleman, L. *J. Am. Chem. Soc.* **2005**, *127*, 15778–15790.
(90) Han, W. G.; Liu, T. Q.; Lovell, T.; Noodleman, L. *Inorg. Chem.* **2006**, *45*, 8533–8542.
(91) Mitić, N.; Clay, M. D.; Saleh, L.; Bollinger, J. M., Jr.; Solomon, E. I. *J. Am. Chem. Soc.* **2007**, *129*, 9049–9065.

JP9033672